Ghost imaging with a SPAD array at low light intensities

V. S. Starovoitov, M. D. Samoilenka, V. N. Chizhevsky

B. I. Stepanov Institute of Physics of the NAS of Belarus, Minsk, Belarus, e-mail: vladstar@ifanbel.bas-net.by

An approach to ghost imaging with a single photon avalanche diode (SPAD) array used simultaneously as a "bucket" detector and an imaging camera is described. The imaging is performed with the help of a pseudo-thermal light source where the light intensity is so low that the dark counts of SPAD have a noticeable effect on imaging. In the approach the data frames are filtered by the number of per-frame counts and the correlation images obtained for different "bucket" pixels are superposed. We demonstrate that the approach is capable to significantly improve image quality.

Keywords: pseudo-thermal light; SPAD array; ghost imaging.

Фантомная визуализация с использованием матрицы детекторов одиночных фотонов при малых интенсивностях света

В. С. Старовойтов, Н. Д. Самойленко, В. Н. Чижевский

Институт физики им. Б. И. Степанова НАН Беларуси, Минск, e-mail: vladstar@ifanbel.bas-net.by

Описана фантомная визуализация (ФВ) объектов при использовании матрицы детекторов одиночных фотонов (SPAD) одновременно как «интегрирующего» детектора, так и визуализирующей камеры. ФВ выполняется для псевдо-теплового излучения малой интенсивности при сильном эффекте темновых отсчетов SPAD. Выполняется фильтрация данных по числу отсчетов в кадре и наложение образов, полученных для различных «интегрирующих» пикселей. Показано, что предложенный подход существенно улучшает качество ФВ.

Ключевые слова: псевдо-тепловое излучение; матрица SPAD; фантомная визуализация.

Introduction

Ghost imaging (GI) is a mature research field dating back nearly a quarter of century. This technique relies on spatial correlations between the two light beams. GI involves a "bucket detector" that measures the total intensity of light after the first light beam passes through an object, and a spatially resolving detector (i. e. an imaging camera) that captures the spatial information of a second (reference) light beam which has never encountered the object. By analyzing the correlated measurements from both detectors, the image of the object can be reconstructed. One of the most perspective ways to enhance GI sensitivity and account for light correlations is to apply recently developed single photon avalanche diode (SPAD) arrays as imaging cameras. In the arrays the image is reconstructed from data (temporal and spatial information for each individual single-pixel detection event) acquired in fixed temporal windows (frames) [1].

In the work, instead of a single-pixel bucket detector, we use several pixels of the imaging SPAD camera (as in [2]) and perform averaging over a ghost images obtained for each "bucket" pixel. Also, we apply frame-filtering of data on the number of counts

per frame We demonstrate that for a standard pseudo-thermal source of correlated photons such an approach can significantly rise the ghost-image quality.

1. Setup and data processing

In the work, the GI is performed by an experiment using light beams produced with help of a laser and a rotating ground-glass disk. The optical layout of the experiment is represented in Fig. 1. The exploited setup and the measurement procedures are described in detail in [2]. The diameter of spot on the rotating disk D illuminated by the Gaussian laser beam is $d_d \approx 0.47$ mm. This spot emits a random structure of light spots (speckles) and is a pseudo-thermal source of correlated photons. The emitted speckles are collected, collimated and then divided by Splitter S₁ into 2 arms: object and reference beams. The reference beam is immediately directed to a SPAD array (A_{SPAD}). The object beam is passed through a target T and then focused onto the same SPAD array. The central part of this focused spot (referred to as "bucket") is used as a bucket detector. The imaged object is the digit template "2" (Element 2 of Group 0) of a 1951 USAF resolution test target. A high-resolution conventional image $I_k^{(r)}$ of this target is depicted in Fig 2, a.

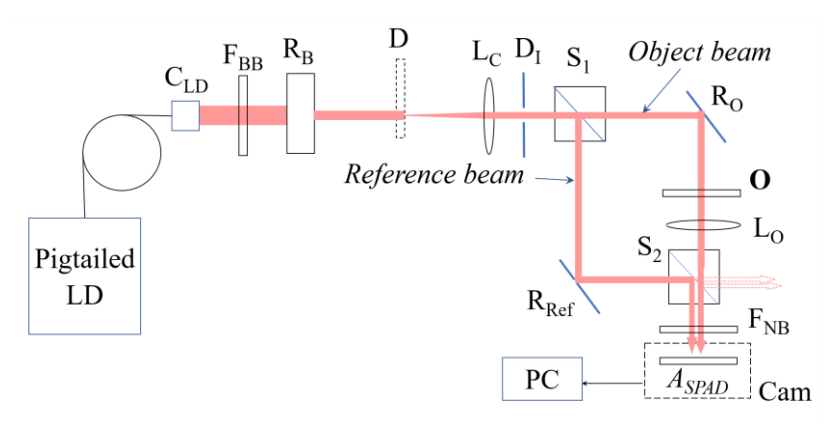


Fig. 1. The optical layout: (LD) laser diode; (C_{LD}) fiber collimator; (F_{BB}) broadband filter; (R_B) beam reducer; (D) rotating ground-glass disk; (L_C , L_T) lenses; (D_I) iris diaphragm; (S_1 , S_2) beam splitters; (R_{Ref} , R_T) mirrors; (T) target; (R_{NB}) narrow-band filter; (R_{SPAD}) SPAD array; (Cam) camera "SuperEllen"; (PC) computer

The SPAD camera is based on the "SuperEllen" sensor, developed by Fondazione Bruno Kessler to quantum imaging applications. The array consists of 32×32 pixels with a pitch of $\delta_s = 44.5 \,\mu\text{m}$ and a total sensitive area of $1.4\times1.4 \,\text{mm}^2$ manufactured in a CMOS standard technology. The pixels are addressed by their linear index $k \in \{1, ..., 1024\}$ such that $k = y_k + 32(x_k - 1)$ where $x_k, y_k \in \{1, ..., 32\}$ are the discrete Cartesian coordinates of pixels. The timestamped counts are registered in a frame-by-frame way.

In our experiment, each frame is a result of light exposition during the time of 45 ns. The data related to an individual frame is converted into a compressed sparse structure $D_f = \{f, n_f, \{x_k^{(i)}, y_k^{(i)}, \tau^{(i)}\}_{i=1,\dots,n_f}\}$ where f is the serial number of frame repetition; n_f is the total number of events (counts) detected by all pixels in frame f; $x_k^{(i)}$, $y_k^{(i)}$, and $\tau^{(i)}$ are the discrete Cartesian coordinates and the detection time for the i-th event registered in frame f. The registered data is collected and transferred to a computer (PC) as a stream of multiple frames $F = \{D_f | n_f \ge 1\}$. The collected data are post processed. At post processing,

both unfiltered and filtered datasets are used. The unfiltered dataset $F_0 = \{D_f | n_f \ge 0\}$ contains all frames registered in the experiment. The total number of frames in this dataset is N_0 . The frame-filtered datasets $F(n^*) = \{D_f | n_f = n^*\}$ are non-overlapping sub-sets of F_0 with fixed number of counts n^* in frame. The prepared dataset is used to calculate both a per-frame distribution of counts and their pairwise correlations [1]

$$G^{(1)}(k) = \langle P_k \rangle_{\{f\}} \text{ and } G^{(1)}(m,k) = \langle P_m P_k \rangle_{\{f\}}, \tag{1}$$

where k and m are linear pixel indices, and $\langle ... \rangle_{ff}$ denotes averaging over the dataset frames. The quantities P_k are random binaries taking the value 1 for a count registration at the pixel k or zero in its absence. In the following consideration we use the normalized second-order correlation function

$$g^{(2)}(m,k) = \frac{G^{(2)}(m,k)}{G^{(1)}(m)G^{(1)}(k)}.$$
 (2)

The ghost image is defined as a weighted sum of several correlation functions

$$I_{k} = \frac{\sum_{m \in \{B\}} G^{(1)}(m) g^{(2)}(m,k)}{\sum_{m \in \{B\}} G^{(1)}(m)},$$
(3)

The pixels labeled by m are "bucket" pixels. The image pixels labeled by k are in the "ghost" area. Quality assessment for the reconstructed ghost images is performed by analyzing the properties of $I_k \equiv I(x_k, y_k)$.

We apply two measures to specify the image quality. First, the contrast-to-noise ratio (CNR defined in [2]) characterizes the quality of spatially restricted image parts. Second, the correlation coefficient R, which pixel-by-pixel measures the strength of linear relationship (that is, a structural similarity) between the analyzed image and a higher-quality reference image $I_k^{(r)}$ of the same object. Unlike CNR, this measure is applicable to the entire image. We apply the correlation coefficient to evaluate the quality for the entire "ghost" area including highly noised pixels.

Overall, at data post-processing, the following procedure of ghost-image reconstruction is implemented. First of all, a dataset (unfiltered F_0) or frame-filtered $(F(n^*))$ is prepared. The prepared dataset is applied to calculate $G^{(1)}(m)$ and $G^{(2)}(m,k)$ and find normalized correlation function $g^{(2)}(m,k)$ (2). Then, a ghost image I_k is computed in accordance with equation (3). Finally, quality of the obtained image is examined visually and estimated using CNR and correlation coefficient R.

2. Results and discussion

In our GI experiment, the light beams are registered under conditions where $\langle n_f \rangle \approx 8$. The maximum count rate for the object-beam spot on the SPAD array is realized near the point (20, 29) (a pixel where the maximal intensity of the object-beam spot is observed). We accept nine low-noise pixels surrounding the point (20, 29) as "bucket" pixels. are used as a set corresponding to the best image reconstruction. The exploited "bucket" pixels are indicated in Fig 2, b. The total number of frames in the unfiltered dataset F_0 is $N_0 \sim 1.9 \times 10^9$. The per-frame probabilities $G^{(1)}(x_k, y_k) \equiv G^{(1)}(k)$ obtained for all pixels of the SPAD array from this dataset are shown in Fig. 2, b.

The computed ghost image $I(x_k,y_k)$ obtained from unfiltered dataset F_0 is represented in Fig. 2, c. This figure shows that the imaged object is recognizable in the

ghost image. However, the presented figure clearly demonstrates drawbacks. The number of noisy pixels is so high that they have a strong destructive effect on the quality of the entire image. According to [2], the efficient number of pixels distinguishable (due to the dark-count effect) in the ghost image reconstructed from the dataset F_0 is of ~ 100 . In addition, the spatial resolution is clearly suffering. The resolution is not high enough to resolve all parts of the object. The "tail" of the imaged digit "2" ($a \sim 0.1$ mm wide strip) is not visible in the reconstructed image. The quality of the obtained image I_k is estimated numerically in terms of CNR and R. The image $CNR \approx 11.7$ is achieved at the contrast of $K \approx 0.101$ and the total error $\sigma \approx 0.0086$. Along our estimation, the coefficient of correlation R between the image I_k and the reference image $I_k^{(r)}$ is of ~ 0.62 . According to the data obtained in [2], the spatial resolution of the image computed from the data F_0 is of $\sim 3.44\delta_s \approx 0.15$ mm.

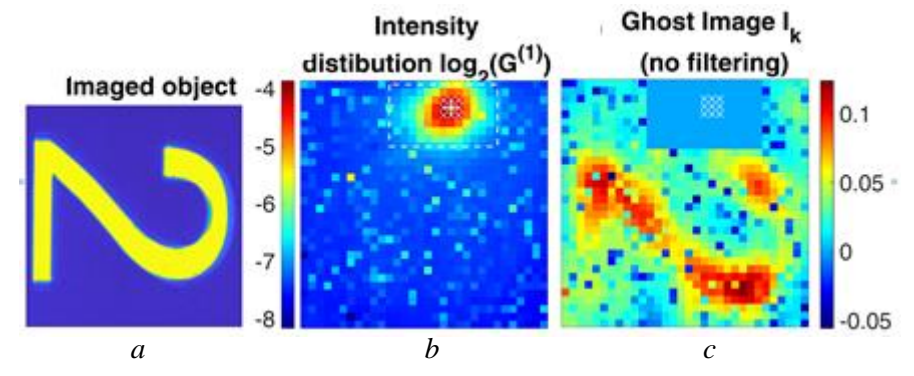


Fig. 2. a – A high-resolution conventional image of the object; b – a typical distribution of $\log_2[G^{(1)}(x_k,y_k)]$; c – a ghost image, obtained for non-filtered dataset F_0

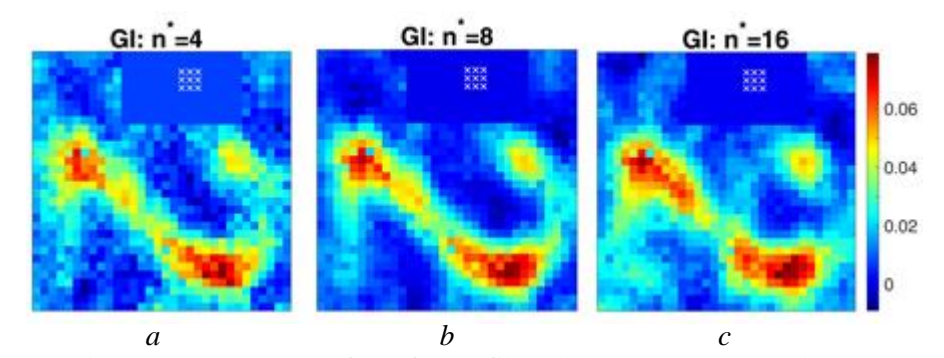


Fig. 3. Ghost images reconstructed from frame-filtered datasets: a - F(4); b - F(8); c - F(16)

We exploit also frame-filtered datasets $F(n^*)$ that are produced by filtering the data F_0 considered in the previous subsection. For the exploited data, the parameter n^* ranges from 2 to 24. Fig. 3 demonstrates images I_k computed from frame-filtered datasets $F(n^*)$ at $n^* = 4$, 8 and 16. In terms of contrast, spatial resolution, and number of distinguishable noised pixels, the presented images look significantly better compared to the ghost image obtained from unfiltered data. Image qualities (such as spatial resolution and contrast) depend on the parameter n^* . Based on visual inspection of the presented images one can conclude that ghost images of the highest quality are realized for datasets $F(n^*)$ with $n^* \sim 8$. As can be seen from Fig. 3, b, the spatial resolution of the image I_k based on the dataset F(8) is high enough to resolve all parts of the imaged object. In accordance with [2] only a few pixels of the image reconstructed from F(8) can be identified as pixels affected by dark counts.

This conclusion is corroborated with the results of numeric evaluation of CNR and the correlation coefficient represented in Fig. 4. Generally, for the ghost image based on the frame-filtered data, the maximum CNR and correlation coefficient R are achieved near those values of $n^* \sim 8$. As shown in Fig. 4 (left Y axis), compared to the "unfiltered" image, the "frame-filtered" image I_k has a higher CNR when the parameter n^* ranges from 5 to 10. At $n^* = 8$, the filtered GI reaches its maximal $CNR \approx 17.0$ which is nearly 45 % higher as compared to the CNR of unfiltered GI. Unlike CNR, the measure of structural similarity R takes into account the effect of strong-noise pixels on the image. Therefore, the range $3 \le n^* \le 19$, where the "low-noise" filtered GI leads to a higher coefficient R (as compared to the "noisy" unfiltered GI), covers almost all of the considered values of n^* . Like CNR, the structural similarity between the reference and ghost images attains its maximum at $n^* = 8$ leading to $R \approx 0.8$ (right Y axis of Fig. 4).

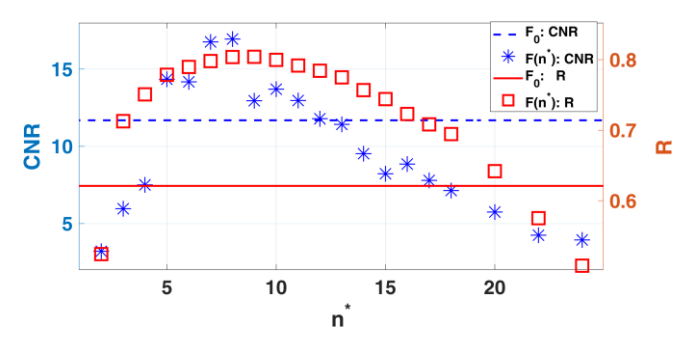


Fig. 4. CNR (left Y axis: blue stars) and correlation coefficient R (right Y axis: red squares) as functions of n^* for ghost images reconstructed from frame-filtered datasets $F(n^*)$. The blue dashed and red solid lines indicate CNR (left Y axis) and R (right Y axis) for the unfiltered data F_0

Conclusion

We have presented an approach to ghost imaging and analyzed the approach capabilities in an experiment where the light intensity is so low that the dark counts have a noticeable effect on the imaging. We have demonstrated that filtering the acquired data with respect to the number of counts per frame and obtaining the image as a weighted average over the images for different "bucket" pixels, one can significantly reduce the destructive effect of dark counts on the ghost image, improve the image contrast, spatial resolution and image similarity to the reference image. The proposed approach allowed us inferring ghost images for dark counts level of 20 % and more of the "bucket" signal level with the photon fluxes of about several photons per time-frame. In our opinion, using multiple bucket detectors instead of just one is compatible with most applications of ghost imaging and will allow one to greatly enhance imaging quality in the extremely-low-light condition. These results can be extended to computational and temporal ghost imaging. Our findings are important for developing correlation imaging schemes with light on a-few-photon level, first of all, for quantum sensing applications.

References

- 1. Spatio-Temporal Correlations of Photons from a Pseudo-Thermal Source / V. S. Starovoitov [at al] // Journal of Applied Spectroscopy 2023. Vol. 90, iss. 2. P. 377–387.
- 2. Frame-filtered ghost imaging with a SPAD array used both as a multiple "bucket" detector and an imaging camera / V. S. Starovoitov [at al] // Applied Optics 2024. Vol. 63, iss. 22. P. 6012–6020.